PHYSICAL REVIEW C VOLUME 24, NUMBER 4 OCTOBER 1981

Optical potential for ^{6}Li elastic scattering at 99 MeV

P. Schwandt, W.W. Jacobs, M.D. Kaitchuck, and P.P. Singh
Indiana University Cyclotron Facility, Bloomington, Indiana 47405

W.D. Ploughe
The Ohio State University, Columbus, Ohio 43212

F.D. Becchetti and J. Jänecke
University of Michigan, Ann Arbor, Michigan 48109
(Received 13 April 1981)

The differential cross section angular distributions for 99-MeV ^{6}Li elastic scattering from ^{12}C, ^{28}Si, ^{40}Ca, ^{58}Ni, ^{90}Zr, and ^{208}Pb have been measured for center-of-mass angles up to $\theta_{max}=43°-69°$. The angular distributions show progressively less structure with increasing target mass which is characteristic of strongly absorbed particles. Phenomenological optical-model analyses with Woods-Saxon form factors exhibit both discrete and continuous ambiguities in the parameters which yield a good fit to the data. The A dependence of several real central potential families and the effects of a surface absorption term have been investigated. A semimicroscopic single-folding ^{6}Li potential based on an $(\alpha+d)$-cluster model for ^{6}Li gave a good description of the data only after renormalization of the real potential by a factor of ~ 0.5.

[NUCLEAR REACTIONS ^{12}C, ^{28}Si, ^{40}Ca, ^{58}Ni, ^{90}Zr, ^{208}Pb (^{6}Li, ^{6}Li), $E_{Li}=99$ MeV: measured elastic scattering $d\sigma/d\Omega$; phenomenological and semimicroscopic optical model analyses.]

I. INTRODUCTION

The study of intermediate energy ^{6}Li elastic scattering and the phenomenological description of differential cross section data is of value because of intrinsic interest in the optical model for strongly absorbed projectiles and because ^{6}Li is the lightest projectile in the transition region between that characteristic of light-ion ($A \leq 4$) and heavy-ion elastic scattering.[1-4] It is, of course, also of practical interest in deducing optical potential parameters for use in distorted wave reaction model calculations. Microscopically, ^{6}Li has presented a problem in the double-folding model description, where the real potential required a normalization of approximately one-half in order to reproduce the data.[2,3] Because of the well-developed cluster structures of ^{6}Li (some with very low binding energies), the importance of various breakup mechanisms in ^{6}Li-induced reactions is also of interest and has been investigated in this region far above the Coulomb barrier.[5]

Previous systematic investigations of ^{6}Li elastic scattering have been made largely at bombarding energies of 50 MeV (Ref. 4) or below, with the exception of a study[1] of ^{6}Li+^{28}Si at 135 MeV. Recently, a study of 154-MeV ^{6}Li+^{28}Si elastic scattering was undertaken,[6] and results on several targets for $E(^6\text{Li})=73.7$MeV (Ref.7) and 88 MeV (Ref. 8) have been obtained. The present results, which have been reported in preliminary form,[9] constitute ^{6}Li elastic scattering data over a wide range of target nuclei, viz., $A=12-208$, for $E_{Li}=99$ MeV. A standard optical-model analysis has been performed and the A dependence of several real central potential families was explored. Along with other recent work, these results should help chart the behavior of ^{6}Li optical-potential parameters with respect to A over a wide range of bombarding energies ($\sim 20-154$ MeV). We have also fitted the data with a semimicroscopic ^{6}Li potential generated using the single-folding approach in an $(\alpha+d)$ cluster representation of ^{6}Li. A substantial renormalization of the real folded potential

is required to fit the data, in remarkably (perhaps fortuitously) good agreement with the results of fully microscopic double-folding approaches.[3]

II. EXPERIMENT

The ^{6}Li beams were provided by the Indiana University Cyclotron Facility (IUCF). Usable intensities of 10–100 nA (electrical) at 99 MeV were achieved by accelerating $^6Li^{++}$ ions through the injector cyclotron and, after further electron stripping, accelerating the bare ^{6}Li ions in the main-stage cyclotron to full energy. Measurements were carried out in the 163-cm diameter IUCF multipurpose scattering chamber. Scattered Li ions were detected and identified in ΔE-E silicon surface barrier detector telescopes (100 μm + 2000 μm0) with angular acceptances of $\sim 1°$. Pulse-height discrimination effectively eliminated all reaction products other than ^{6}Li and ^{7}Li. With the exception of ^{208}Pb, the (^{6}Li,^{7}Li) reaction Q values were sufficiently negative for the targets studied that more sophisticated particle-identification techniques were not needed. Isotopically enriched targets (except for Si) of thicknesses ranging from 11 to 33 mg/cm^2 were used. The overall energy resolution in these measurements was typically 300–500 keV.

Solid-state detectors mounted out of the reaction plane at symmetric forward angles to the left and right of the beam were used to monitor the product of beam flux times target thickness. In addition, these counters were placed at angles where the cross sections change fairly rapidly, and were thus useful for monitoring angular and positional stability of the beam on target. The nominal 0° reference of the beam was deduced from measurements made on either side of the beam with the detector telescopes with an estimated uncertainty of $\pm 0.05°$.

III. RESULTS

The differential cross sections are plotted in Fig. 1. Except for ^{12}C, measurements were made for each target until the cross section was on the order of 10 μb/sr. At the forward angles, the data, including angular uncertainties, were reproducible to the level of $\pm 3\%$ to $\pm 5\%$ with minimal statistical uncertainties. The relative uncertainty in the more backward angle points is dominated by statistics and ranges from $\pm 5\%$ to $\pm 10\%$ ($\pm 15\%$ for the very last data points). Absolute errors are estimated to be $\pm 12\%$, and are due largely to target thickness uncertainties.

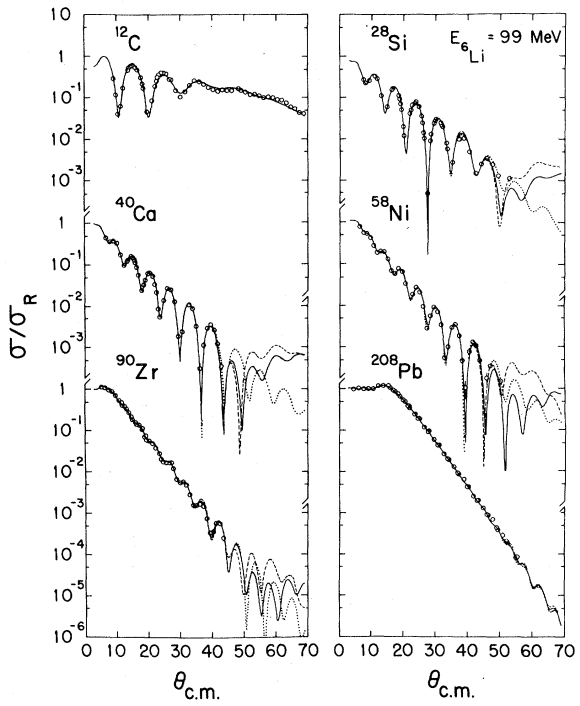

FIG. 1. Differential cross section angular distributions, plotted as ratio-to-Rutherford, for 99 MeV ^{6}Li elastic scattering from various targets. Except where indicated, the relative (statistical) errors are smaller than the plotted points. The curves are the results of an optical model analysis as described in the text, with the dotted, solid, and dashed lines corresponding to potential families I, II, and III, respectively.

The absolute elastic cross sections for the ^{58}Ni, ^{90}Zr, and ^{208}Pb targets span a range of values covering 7 to 8 decades over the angular range measured, corresponding to an average rate of falloff by a factor of 10 over 8° to 6° intervals. For the lighter mass targets ($A \lesssim 30$), the ^{6}Li elastic scattering exhibits forward-angle diffractive oscillations which die out somewhat with increasing angle. In contrast, for the heavier targets ($A \gtrsim 60$), the forward-angle data beyond the Coulomb-nuclear interference "knee" start out as a relatively smooth exponential falloff, with increasingly pronounced oscillatory structure appearing at larger angles. These general features are typical of the scattering of strongly absorbed ions and can be characterized by two parameters and their corresponding features: the Sommerfeld parameter η, which characterizes the Coulomb interaction, and the critical angular momentum λ, for which the modulus of the S matrix is $|S_\lambda| = 0.5$, and which

characterizes strong absorption. For $\lambda >> 1\hbar$, the nuclear scattering is diffractive. This condition is fulfilled for all of the present data where $\lambda = 28\hbar$ and $50\hbar$ for Si and Pb, respectively. The nature of the diffractive scattering, Fraunhofer or Fresnel, depends on whether the Coulomb interaction satisfies the condition p << 1 (Fraunhofer diffraction) or $p >> 1$ (Fresnel diffraction), where $p \equiv 2\eta [1-(2E/V-1)^{-2}]$. For the present ^{6}Li experiment, $p=3$ for Si and $p=13$ for Pb. The scattering from Pb and Zr at this energy is therefore qualitatively of the Fresnel type with a typical structureless exponential falloff of σ/σ_R with scattering angle (i.e., contributions from only one side of the large absorptive nuclear disc are seen). For the lightest targets one observes Fraunhofer oscillations at the forward angles where contributions from opposite sides of the interaction region interfere; with increasing Coulomb barrier these oscillations move to larger angles because of the "diverging lens" effect of the repulsive Coulomb field. The disappearance of Fraunhofer diffraction at the larger angles for the lightest targets signals the change from peripheral diffractive scattering to smooth refractive scattering from the nuclear interior.

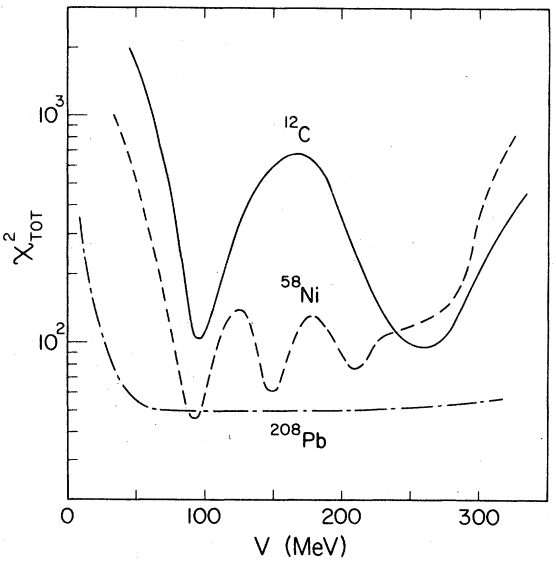

FIG. 2. Quality-of-fit parameter $(\chi^2)_{tot}$ versus the strength V of the real central potential following a search on all other potential parameters. The large variation in spacing between potential families for ^{12}C and ^{58}Ni was characteristic of all targets studied with the exception of ^{208}Pb which shows little sensitivity to changes in V.

IV. OPTICAL MODEL ANALYSES

A. Phenomenological optical potential

The angular distributions were fitted using the code SNOOPY[10] and an optical potential of conventional form, containing a Coulomb term and a complex nuclear central term

$$U(R) = U_{\text{Coul}}(R) - Vf_o(R) - i(W_S - 4a_w W_D d/dR) f_w(R) \quad (1)$$

with Woods-Saxon form factors $f_x(R;r_x,a_x) = \{1+\exp[(R-r_x A^{1/3})/a_x]\}^{-1}$ and six free parameters (with either W_D or W_S set equal to zero). Although a calculation with a double-folding model spin-orbit potential has been found to give a good description of some ^{6}Li analyzing power data,[11] the inclusion of such a spin-orbit term in fitting cross section data alone has been shown to have little effect[3] and for that reason was ignored in the present analysis.

The discrete potential strength ambiguities commonly encountered for moderately or strongly absorbed projectiles at lower energies are still unresolved by the present higher-energy data. This behavior is displayed in Fig. 2 for several representative targets. One also sees clearly the A dependence of the real potential depth for a given family. The lack of any oscillatory structure in the ^{208}Pb angular distribution makes it insensitive to changes in V. With the exception of ^{208}Pb, more extensive searches were carried out for each target near the χ^2 minima. The parameters resulting from such a search, using a volume absorption term, are listed in Table I for the different families (sets I–IV). Figure 3 illustrates the behavior of V for the various potential sets versus $A^{1/3}$. The dashed lines in the figure indicate the extrapolation made to select an appropriate potential strength for ^{208}Pb in each case. The "preferred" (for reasons discussed below) parameter set II is emphasized in this figure by a heavy line.

Calculations for potential sets I–III are shown with the differential cross section data in Fig. 1. Only at the more backward angles are any differences between the calculations discernible, the deeper potentials yielding the larger cross sections. Although there is some slight preference in terms of χ^2 for the set $V \sim 95$ MeV at $E(^6\text{Li}) = 99$ MeV, parameter set II is the one which is compatible with the 154-MeV ^{6}Li+^{28}Si results[6] which selected a "unique" potential $V \sim 160$ MeV and for this reason is considered the preferred parameter set. The effect of a surface, rather than volume, absorption term was investigated for this latter set, using

TABLE I. Optical potential parameter sets for various families of real central potentials (potential strengths in MeV, geometry parameters in fm). Also listed are the χ^2 per point, the reaction cross section (in mb), and potential volume integrals in (MeV fm^3).

	Set	V	r_0[a]	a_0	W_S	r_w[a]	a_w	χ^2/N	σ_R	$J_R/6A$	$J_I/6A$
^{12}C	I	105	1.278	0.800	44.7	1.259	1.114	1.89	1444	267	156
	II	260	0.953	0.800	58.6	1.051	1.158	1.74	1463	368	160
	III	510	0.716	0.800	69.4	0.944	1.170	1.87	1468	449	165
^{28}Si	I	92	1.308	0.840	22.9	1.825	0.761	2.23	1669	207	115
	II	175	1.122	0.840	27.5	1.759	0.779	2.69	1675	276	126
	III	270	0.997	0.840	28.9	1.744	0.781	2.96	1676	330	130
^{40}Ca	I	92	1.302	0.879	18.4	1.885	0.707	1.73	1883	196	96
	II	152	1.169	0.877	17.6	1.892	0.726	2.20	1903	250	94
	III	225	1.066	0.875	18.1	1.879	0.738	2.71	1911	299	95
^{58}Ni	I	94	1.304	0.865	21.0	1.732	0.773	1.22	2098	188	86
	II	147	1.196	0.865	21.4	1.721	0.792	1.49	2115	236	87
	III	195	1.133	0.865	24.7	1.678	0.797	2.24	2102	274	94
^{90}Zr	I	94	1.302	0.842	20.5	1.683	0.804	0.92	2455	175	76
	II	134	1.228	0.845	21.6	1.669	0.817	0.89	2468	213	78
	III	174	1.174	0.848	22.2	1.664	0.822	0.92	2478	247	80
	IV	214	1.134	0.849	23.0	1.652	0.823	1.10	2470	278	81
^{208}Pb	I	95	1.274	0.871	23.5	1.538	0.806	0.92	2912	155	64
	II	125	1.230	0.875	24.7	1.528	0.813	0.93	2917	186	67
	III	155	1.198	0.875	25.0	1.525	0.815	0.94	2917	214	67
	IV	185	1.174	0.875	25.0	1.525	0.815	1.03	2919	242	67

[a]Radii defined by $R_i = r_i A^{1/3}$, where A is the target mass number.

starting values from Table I and searching on all parameters with the exception of V. The results are given in Table II; the fits are similar in quality (although slightly but not significantly worse overall in terms of χ^2) to those obtained with the volume absorption term. This result is not too surprising. Using a "notch-perturbation" test,[12] we find that even at this elevated energy, ^{6}Li scattering forward of 70° is still sensitive predominantly to the nuclear potential in the surface region, largely beyond the half-density point.

B. Single-folding cluster-model potential

In view of the appreciable cluster probability of ^{6}Li as a weakly-bound $\alpha+d$ system, we have also attempted to describe the ^{6}Li elastic scattering within the framework of a simple cluster potential folding model. In terms of the well-known α-particle and deuteron optical potentials, U_α and U_d, we define the ^{6}Li optical potential as

$$U_{^6\mathrm{Li}}(R) = \int \{ U_\alpha(|\vec{\mathrm{R}} - \vec{\mathrm{r}}/3|) + U_d(|\vec{\mathrm{R}} - 2\vec{\mathrm{r}}/3|) \} \times |X_{\alpha d}(r)|^2 d\vec{\mathrm{r}}, \quad (2)$$

where $X_{\alpha d}$ is the intercluster (α-d relative motion) function. Ignoring possible distortion of the cluster and its constituents in the nuclear field, we generated reasonable S-state model wave functions $X_{\alpha d}$ from phenomenological $\alpha+d$ potentials which were required to reproduce correctly (1) the binding energy $E_B = 1.472$ MeV of ^{6}Li with respect to breakup into $\alpha+d$, (2) the empirical low-energy $^3S_1$ α-d scattering phase shifts,[13] and (3) the charge form factor of the ^{6}Li ground state as determined from electron scattering.[14] Furthermore, in order to account phenomenologically for antisymmetrization effects at small α-d separation distances r, we required $X_{\alpha d}$ to have the correct radial quantum number (e.g., a $2S$ state) and/or approach zero faster than r^2 as $r \to 0$ (e.g., by introducing a repulsive core in the potential). Two possible α-d bound

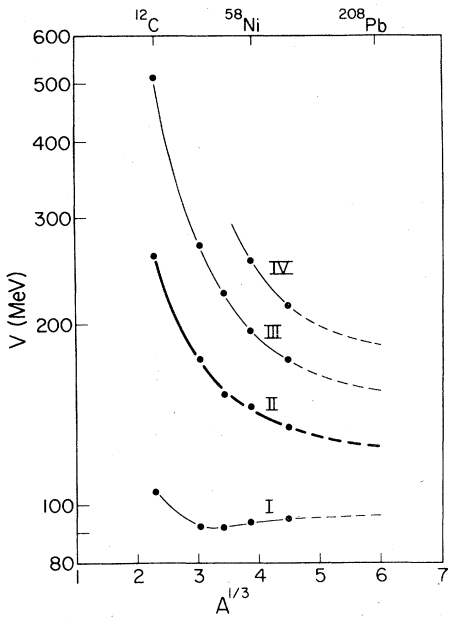

FIG. 3. Variation of the strength V of the real central potential versus $A^{1/3}$ for the various potential families I–IV as described in the text. The heavy line shows the behavior with target mass for the family preferred by higher energy measurements.[6] The dashed line in all cases shows the extrapolation of these parameter values to the ^{208}Pb region, where little sensitivity to variation of V is observed.

state form factors were chosen to investigate the sensitivity of the folded ^{6}Li potential to the choice of $X_{\alpha d}$. One choice (a) represents a $2S$ state (with a node at 1.6 fm) in a real Woods-Saxon plus Coulomb potential,[15]

$$V_{\alpha d}(r) = -V_o\{1+\exp[(r-R)/a]\}^{-1} + V_C(r)$$

with $V_o = 79.0$ MeV, $R = 1.83$ fm, $a = 0.70$ fm, and $V_C(r)$ due to a uniformly charged sphere of radius R. The second choice (b) is a node-free $1S$ Eckart function $N(1-e^{-\alpha r})^3(1/r)e^{-kr}$, with $\alpha = 0.714$ fm^{-1} and $k^2 \equiv 2\mu E_B/\hbar^2$, which is an eigenstate of the real potential with repulsive core, $V_{\alpha d}(r) = -[44.4(e^{\alpha r}-1)^{-1} - 47.5(e^{\alpha r}-1)^{-2}]$ MeV.[16] [For a recent discussion of these and alternative α-d bound state form factors and their relevance to $(d,^6\text{Li})$ α-transfer reactions, see Ref. 17.]

For U_α and U_d we chose phenomenological optical potentials[18] which fit elastic α and d scattering data at the appropriate energies $E_\alpha \simeq 2/3E_{\text{Li}}$ and $E_d \simeq 1/3E_{\text{Li}}$. For ^{58}Ni, the resulting folded ^{6}Li potential (real and imaginary central parts) is compared to the best-fit phenomenological Woods-Saxon potential in Fig. 4. The ^{6}Li folded potential is seen to be fairly insensitive to the particular choice of the intercluster function $X_{\alpha d}$. The generally good overall agreement of the imaginary potentials is very likely fortuitous since absorption modes clearly exist for ^{6}Li which cannot be accounted for by the superposition of α-particle and deuteron absorption. The real part of the folded ^{6}Li potential agrees remarkably well in *shape* with the phenomenological real potential, but is clearly too large in *magnitude* by about a factor of 2 everywhere, including the all-important surface region $4 < R < 7$ fm. Such a large and systematic overestimate of the real potential for ^{6}Li by the $\alpha+d$ cluster folding model has also been found consistently[2,3,8] for the double-folding model of the ^{6}Li potential in terms of an effective two-nucleon interaction which gives a reasonable account of the scattering of heavier projectiles.

We fit the 99-MeV ^{6}Li elastic scattering data with the single-folded potential, freely renormalized by a factor N, using two forms of the imaginary potential: (1) the folded imaginary form factor with strength adjusted for best two-parameter fit, and (2) a Woods-Saxon imaginary potential with adjustable parameters (four-parameter fit). The

TABLE II. Optical potential parameters for set II with surface absorption (potential strengths in MeV, geometry parameters in fm). Also listed are the χ^2 per point, the reaction cross section (in mb), and the potential volume integrals (in MeV fm^3).

	V	r_0[a]	a_0	W_D	r_w[a]	a_w	χ^2/N	σ_R	$J_R/6A$	$J_I/6A$
^{12}C	260	0.953	0.800	37.6	0.534	1.179	1.93	1474	369	160
^{28}Si	175	1.125	0.840	39.0	1.262	0.798	2.98	1665	278	156
^{40}Ca	152	1.200	0.844	31.0	1.360	0.791	4.61	1895	260	122
^{58}Ni	147	1.213	0.843	36.0	1.256	0.826	2.59	2083	241	111
^{90}Zr	134	1.221	0.844	31.0	1.284	0.856	0.91	2438	210	88
^{208}Pb	125	1.206	0.905	37.0	1.243	0.848	0.83	2908	177	72

[a]Radii defined by $R_i = r_i A^{1/3}$, where A is the target mass number.

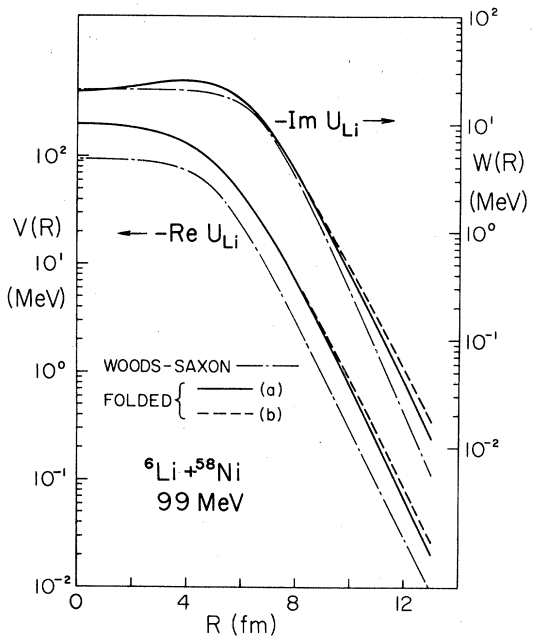

FIG. 4. Comparison of phenomenological Woods-Saxon real and imaginary potentials with single-folding cluster-model potentials. The solid and dashed lines represent calculations employing two different $\alpha-d$ bound state form factors as described in the text.

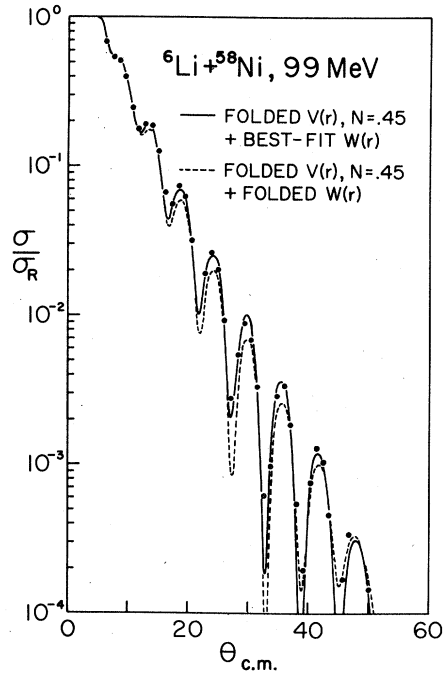

FIG. 5. Fit to the 99-MeV ^{6}Li+^{58}Ni elastic scattering data with a real folded potential (renormalized by a factor N) and two forms of the imaginary potential as described in the text.

results are illustrated in Fig. 5 for the representative case of ^{58}Ni. A good fit is obtained in the latter case with $N=0.45$ and a Woods-Saxon imaginary potential (solid curve); the χ^2 is about twice that for the purely phenomenological potential-model fit. The fit obtained with the folded imaginary potential (dashed curve) is considerably worse, with a χ^2 value which is seven times larger than the best-fit χ^2 value.

V. DISCUSSION AND CONCLUSIONS

Differential cross sections for ^{6}Li elastic scattering at 99 MeV from targets in a wide mass range have been measured. These data are described quite well in terms of a conventional optical-model potential with Woods-Saxon form factors. The model parameters exhibit both discrete and continuous ambiguities. Of various real-well potential families which were found to describe the data, one set in particular (II) is in good agreement with the real potential strength V selected by higher-energy ^{6}Li elastic scattering.[6]

We also find here the same systematic features of the potential parameters observed for ^{6}Li elastic scattering at neighboring energies,[6,8] namely large values of a_o, r_w, and a_w, which are characteristic of ^{6}Li but not typical of heavier ions. These parametric values reflect the general observation that for ^{6}Li the imaginary potential effectively dominates the real potential beyond the strong-absorption radius, while the reverse situation holds true in the nuclear interior. This is in contrast to medium-energy scattering of ^{4}He, for which $\mathrm{Re}U >> \mathrm{Im}U$ at all radii, and of ^{12}C (for example) for which $\mathrm{Im}U > \mathrm{Re}U$ at all radii. The peculiar surface behavior for ^{6}Li may well be indicative of the ease with which ^{6}Li, unlike ^{4}He or ^{12}C, breaks up in the Coulomb and nuclear fields.

A semimicroscopic approach to generating the ^{6}Li potential in an $\alpha+d$ cluster model by single folding of the appropriate empirical α-particle and deuteron optical potentials gives a satisfactory representation of the ^{6}Li data only after renormalization of the real folded potential strength by a factor $N\sim0.5$ on the average. This result is consistent with a similar renormalization ($N \sim 0.6$) found necessary in fully-microscopic double-folding potential descriptions of ^{6}Li elastic scattering at similar or lower energies.[2,3,8]

The above close agreement of normalization factors may well be fortuitous since the possible causes for renormalization are likely to be different

for the two very different folding-model approaches. In the present single-folding model calculations, we have assumed an $\alpha+d$ cluster probability $P_{\alpha d}=1.0$, while experimental evidence from various ^{6}Li reactions and theoretical models of the ^{6}Li ground state suggest $P_{\alpha d}\sim 0.7$. On one hand, the $\alpha+d$ cluster contribution to the ^{6}Li potential should then be reduced by $\sim 30\%$; on the other hand, a number of other contributions which have been neglected should then be included, such as the effect of other cluster configurations, D-state components, dynamic distortion of the cluster wave functions, etc. How the various approximations and/or missing pieces affect N is not obvious.

It seems reasonable, however, to ascribe a significant portion of the renormalization in both folding models to the polarization and breakup of ^{6}Li, or its consituent clusters, in the field of the target nucleus, but no theoretical calculations of these effects have yet been made. The recent explanation[19] of a similar renormalization problem in the ^{7}Li and ^{9}Be double-folding model calculations in terms of the large projectile quadrupole moments does not affect the ^{6}Li anomaly since the latter ion has a very small quadrupole moment. It has been suggested[19] that in the ^{6}Li case, coupling to the strongly-excited 3^+(2.18 MeV) state in ^{6}Li could play a similar role.

ACKNOWLEDGMENTS

We thank Mr. Jon Meek and Dr. A. Nadasen for generous help during the early data taking. This work was supported in part by the National Science Foundation under grants PHY-76-84033 (IUCF), and PHY-78-07754 (University of Michigan).

[1]R.M. DeVries, D.A. Goldberg, J.W. Watson, M.S. Zisman, and J.G. Cramer, Phys. Rev. Lett. 39, 450 (1977).
[2]G.R. Satchler and W.G. Love, Phys. Lett. 76B, 23 (1978).
[3]D.P. Stanley, F. Petrovich, and P. Schwandt, Phys. Rev. C 22, 1357 (1980).
[4]L.T. Chua, F.D. Becchetti, J. Jänecke, and F.L. Milder, Nucl. Phys. A273, 243 (1976).
[5]C.M. Castaneda, H.A. Smith, P.P. Singh, and H. Karwowski, Phys. Rev. C 21, 179 (1980).
[6]P. Schwandt, S. Kailas, W.W. Jacobs, M.D. Kaitchuck, W. Ploughe, and P.P. Singh, Phys. Rev. C 21, 1656 (1980).
[7]R. Huffman, A. Galonsky, R. Markham, and C. Williamson, Phys. Rev. C 22, 1522 (1980).
[8]C.B. Fulmer, G.R. Satchler, E.E. Gross, F.E. Bertrand, C.D. Goodman, D.C. Hensley, J.R. Wu, N.M. Clarke, and M.F. Steeden, Nucl. Phys. A356, 235 (1981).
[9]P. Schwandt, P.P. Singh, A. Nadasen, G. Adams, F.D. Becchetti, J. Jänecke, and W. Ploughe, Bull. Am. Phys. Soc. 22, 633 (1977).
[10]P. Schwandt, Indiana University Cyclotron Facility Internal Report 77-8 (unpublished), p. 85.
[11]F. Petrovich, D. Stanley, L.A. Parks, and P. Nagel, Phys. Rev. C 17, 1642 (1978).
[12]J.G. Cramer and R.M. DeVries, Phys. Rev. C 22, 91 (1980).
[13]L.C. McIntyre and W. Haeberli, Nucl. Phys. 91, 382 (1967).
[14]G.C. Li, I. Sick, R.R. Whitney, and M.R. Yearian, Nucl. Phys. A162, 583 (1971).
[15]G.R. Plattner, M. Bornand, and K. Alder, Phys. Lett. 61B, 21 (1976).
[16]J.V. Noble, Phys. Rev. C 1, 1900 (1970).
[17]J. Jänecke, F.D. Becchetti, and D. Overway, Nucl. Phys. A343, 161 (1980).
[18]W.W. Daehnick, J. Childs, and Z. Vrcelj, Phys. Rev. C 21, 2253 (1980); H.H. Chang *et al.*, Nucl. Phys. A270, 413 (1976); L.W. Put and A.M.J. Paans, *ibid.* A291, 93 (1977).
[19]V. Hnizdo, K.W. Kemper, and J. Szymakowski, Phys. Rev. Lett. 46, 590 (1981).